Available online at www.sciencedirect.com
ScienceDirect
Spectrochimica Acta Part A 71 (2008) 252–262
SPECTROCHIMICA ACTA PART A
www.elsevier.com/locate/saa

Analysis of vibrational spectra of L-alanylglycine based on density functional theory calculations

L. Padmaja [a,1], C. Ravikumar [a], C. James [b], V.S. Jayakumar [a], I. Hubert Joe [a,*]

[a] *Centre for Molecular and Biophysics Research, Department of Physics, Mar Ivanios College, Thiruvananthapuram 695 015, Kerala, India*
[b] *Department of Physics, Scott Christian College, Nagercoil 629 003, Tamilnadu, India*

Received 27 June 2007; received in revised form 10 December 2007; accepted 14 December 2007

Abstract

FT Raman and IR spectra of the crystallized biologically active molecule, L-alanylglycine (L-Ala-Gly) have been recorded and analyzed. The equilibrium geometry, bonding features and harmonic vibrational frequencies of L-Ala-Gly have been investigated with the help of B3LYP density functional theory (DFT) method. The calculated molecular geometry has been compared with the experimental data. The assignments of the vibrational spectra have been carried out with the help of normal coordinate analysis (NCA) following the scaled quantum mechanical force field methodology (SQMFF). The optimized geometry shows the non-planarity of the peptide group of the molecule. Potential energy surface (PES) scan studies has also been carried out by *ab initio* calculations with B3LYP/6-311+G** basis set. The red shifting of NH_3^+ stretching wavenumber indicates the formation of N—H···O hydrogen bonding. The change in electron density (ED) in the σ^* antibonding orbitals and E2 energies have been calculated by natural bond orbital analysis (NBO) using DFT method. The NBO analysis confirms the occurrence of strong intermolecular hydrogen bonding in the molecule.

Keywords: DFT; Normal coordinate analysis; PES scan; NBO analysis; PED

1. Introduction

Amino acids are the fundamental building blocks of proteins. Basically, amino acids are joined together by peptide bonds to form the basic structure of proteins. L-alanine is the smallest physically occurring chiral amino acid. In crystalline state it serves as model for an examination of an extensive range of intermolecular interactions of importance in chemistry and biology [1]. Traditionally glycine has been used for the treatment of stomach ulcers caused by excessive stomach acid. Glycine has also been proved to be potential drug in healing injuries to skin, connective tissues and production of bile salts which are important for digestion, particularly of fats. Glycine is also a component of glucose tolerance factor which helps insulin stabilize blood sugar [2–5].

Spectroscopic techniques are capable of giving a detailed awareness of any molecular framework. Infrared and Raman spectra in conjunction with quantum chemical computations, lead to precise information about the structure of molecules. These spectroscopic methods is an effective approach to describe the nature of chemical bonds involved, the behavior of normal modes and the effect of various types of intermolecular forces. Studies of amino acids by vibrational spectroscopy are very much useful in obtaining information regarding the molecular confirmation and the nature of hydrogen bonding in biologically important substances [6,7]. In this present study, a detailed vibrational spectral investigation of L-alanylglycine (L-Ala-Gly) has been performed using the scaled quantum mechanical (SQM) force field technique based on density functional theory (DFT) calculations.

2. Experimental

2.1. Synthesis

The title compound L-Ala-Gly was grown by slow evaporation at room temperature of an aqueous solution containing L-alanine and glycine in 1:1 stoichiometric ratio. Koch and Germain [8] reported the crystal structure of L-Ala-Gly. Amino acids

* Corresponding author. Tel.: +91 4712351053.
E-mail address: hubertjoe@sancharnet.in (I. Hubert Joe).
[1] Permanent address: Department of Physics, Nesamony Memorial Christian College, Marthandam 629 165, Tamil Nadu, India.

1386-1425/$ – see front matter © 2008 Elsevier B.V. All rights reserved.
doi:10.1016/j.saa.2007.12.019

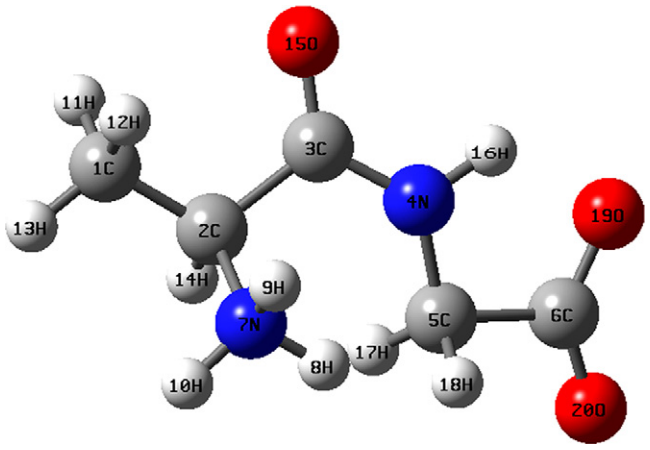

Fig. 1. Optimized structure of L-Ala-Gly.

can combine easily by removing a water molecule, joining the amino end of one amino acid with the carboxyl end of another. The method of peptide bond creation is identical to the process of condensation polymerization forming nylon [9]. In the similar manner, the amino acids L-alanine and glycine can combine to form a dipeptide, L-alanylglycine.

2.2. IR and Raman measurements

The FT-IR spectrum of L-Ala-Gly was recorded in the region 4000–400 cm^{-1}, with samples in the KBr pellet, using Nicolet Magna 560 FT-IR spectrometer. The resolution of the spectrum is 4 cm^{-1}.

The NIR-FT Raman spectrum of L-Ala-Gly crystal was obtained in the range 3200–600 cm^{-1} using Bruker RFS 100/S FT Raman spectrophotometer with a 1064 nm Nd: YAG laser source of 100 mW power. Liquid nitrogen cooled Ge-diode was used as a detector. Spectra were collected for samples with 1000 scan accumulated for over 30 min duration. The spectral resolution after apodization was 2 cm^{-1}. A correction according to the fourth power scattering factor was performed, but no correction to instrumental was done. The upper limit for the wavenumber is 3500 cm^{-1} due to the detector sensitivity and the lower one is around 10 cm^{-1} due to the Rayleigh line cut off by a notch filter.

3. Computational details

The quantum chemical computations of L-Ala-Gly has been performed using Gaussian 98 program package [10] at the Becke3–Lee–Yang–Parr (B3LYP) level with standard 6-31G* and 6-311+G** basis sets. The optimized geometry corresponding to the minimum on the potential energy surface has been obtained by solving self-consistent field equation iteratively. The harmonic vibrational frequencies have been analytically calculated by taking the second order derivative of energy using the similar level of theory. Multiple scaling of the force field has been performed by the SQM procedure [11,12] to offset the systematic errors caused by basis set incompleteness, neglect of electron correlation and vibrational anharmonicity [13]. Normal coordinate analysis has been performed to obtain full description of the molecular motion pertaining to the normal modes using the MOLVIB program version 7.0 written by Sundius [14,15]. The Raman activities (S_i) calculated by Gaussian 98 program have been suitably adjusted by the scaling procedure with MOLVIB and subsequently converted to relative Raman intensities (I_i) using the following relationship derived from the basic theory of Raman scattering [16,17]

$$I_i \frac{f(\nu_o - \nu_i)^4 S_i}{\nu_i[1 - \exp(-hc\nu_i/kT)]}, \quad (1)$$

Table 1a
Optimized bond lengths (Å) of L-Ala-Gly on B3LYP/6-311+G** basis set

Parameter	Monomer	Dimer	Expt.[a]
C_1—C_2	1.52	1.52	1.51
C_2—C_3	1.56	1.51	1.52
C_3—N_4	1.34	1.36	1.33
N_4—C_5	1.46	1.46	1.44
C_5—C_6	1.61	1.55	1.52
C_2—N_7	1.53	1.50	1.49
N_7—H_8	1.04	1.08	–
N_7—H_9	1.02	1.05	–
N_7—H_{10}	1.02	1.02	–
C_1—H_{11}	1.09	1.10	–
C_1—H_{12}	1.09	1.09	–
C_1—H_{13}	1.09	1.09	–
C_2—H_{14}	1.09	1.09	–
C_3—O_{15}	1.22	1.23	1.22
N_4—H_{16}	1.03	1.01	–
C_5—H_{17}	1.09	1.09	–
C_5—H_{18}	1.10	1.10	–
C_6—O_{19}	1.25	1.28	1.26
C_6—O_{20}	1.23	1.25	1.24

[a] Taken from Ref. [4].

Table 1b
Optimized bond angles (°) of L-Ala-Gly on B3LYP/6-311+G** basis set

Parameter	Monomer	Dimer	Expt.[a]
C_1—C_2—C_3	113.4	112.2	111.0
C_2—C_3—N_4	115.1	118.2	114.3
C_3—N_4—C_5	130.0	128.2	120.2
N_4—C_5—C_6	108.3	117.6	114.2
C_1—C_2—N_7	110.0	110.8	109.6
C_3—C_2—N_7	107.0	103.8	108.4
C_2—N_7—H_8	108.6	109.3	–
C_2—N_7—H_9	110.3	104.3	–
C_2—N_7—H_{10}	112.2	113.1	–
C_2—C_1—H_{11}	108.6	110.6	–
C_2—C_1—H_{12}	111.4	109.8	–
C_2—C_1—H_{13}	111.5	110.2	–
C_1—C_2—H_{14}	111.5	110.8	–
C_2—C_3—O_{15}	118.4	118.3	121.6
N_4—C_3—O_{15}	126.5	122.7	124.0
C_3—N_4—H_{16}	119.3	112.1	–
N_4—C_5—H_{17}	113.3	107.6	–
N_4—C_5—H_{18}	113.2	110.5	–
C_5—C_6—O_{19}	112.9	114.0	115.8
C_5—C_6—O_{20}	112.9	119.0	119.9

[a] Taken from Ref. [4].

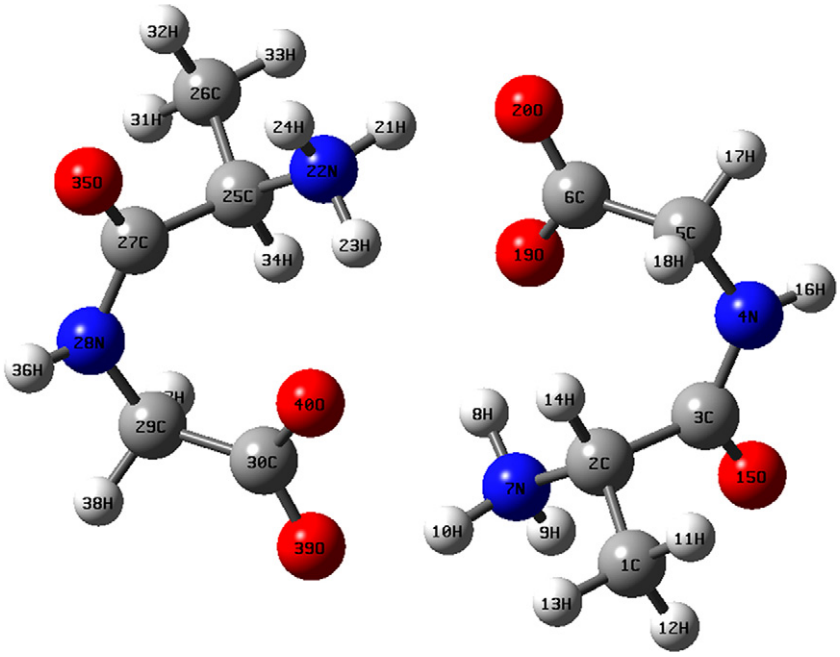

Fig. 2. Optimized structure of L-Ala-Gly dimer.

where ν_o is the exciting frequency (in cm^{-1}), ν_i is the vibrational wavenumber of the ith normal mode, h, c and k are universal constants, and f is the suitably chosen common scaling factor for all the peak intensities. For simulation of calculated IR and Raman spectra have been plotted using pure Lorentzian band shapes with a bandwidth of (FWHM) of 10 cm^{-1}.

4. Results and discussion

4.1. Optimized geometry

The optimized molecular structure of L-Ala-Gly monomer (Fig. 1) and dimer (Fig. 2) determined using Gaussian 98W program. The optimized geometry is summarized in Table 1 with the comparison of experimental values [8]. From the geometry, the bond distance of C_3–O_{15} is small compared with other C–O bonds. The calculated bond angle N_4–C_3–O_{15} is larger than the experimental value by nearly 2.5°. The lowering of C_3–O_{15} bond length and the increasing of bond angle N_4–C_3–O_{15} is due to the oxygen of the peptic group is not implemented in any hydrogen link [8]. The calculated bond length of C_6–O_{19} and C_6–O_{20} of the carboxyl group is 1.25 and 1.23 Å. This difference in bond length between the two links C–O of the carboxyl group is due to different environment of oxygen. The predicted bond lengths of C_1–C_2, C_2–N_7, C_2–C_3, C_3–N_4, N_4–C_5 and C_5–C_6 are elongated by 0.01, 0.04, 0.04, 0.01, 0.02 and 0.09 Å, respectively, from the

Table 1c
Optimized dihedral angles (°) of L-Ala-Gly on B3LYP/6-311+G** basis set

Parameter	Monomer	Dimer
C_1–C_2–C_3–N_4	174.6	−131.2
C_2–C_3–N_4–C_5	15.1	−11.4
C_3–N_4–C_5–C_6	156.7	−61.0
N_4–C_3–C_2–N_7	53.1	−131.2
C_3–C_2–N_7–H_8	−57.4	−50.3
C_3–C_2–N_7–H_9	60.9	68.9
C_3–C_2–N_7–H_{10}	−178.2	−171.9
C_3–C_2–C_1–H_{11}	60.8	−62.2
C_3–C_2–C_1–H_{12}	−56.5	55.1
C_3–C_2–C_1–H_{13}	−179.9	180.0
N_4–C_3–C_2–H_{14}	−59.8	−4.1
C_1–C_2–C_3–O_{15}	−3.2	51.0
C_6–C_5–N_4–H_{16}	−3.7	99.4
C_2–C_3–N_4–H_{16}	173.6	−172.6
C_3–N_4–C_5–H_{17}	37.3	176.9
C_3–N_4–C_5–H_{18}	−89.0	61.9
N_4–C_5–C_6–O_{19}	1.90	10.8
N_4–C_5–C_6–O_{20}	−178.8	−172.2

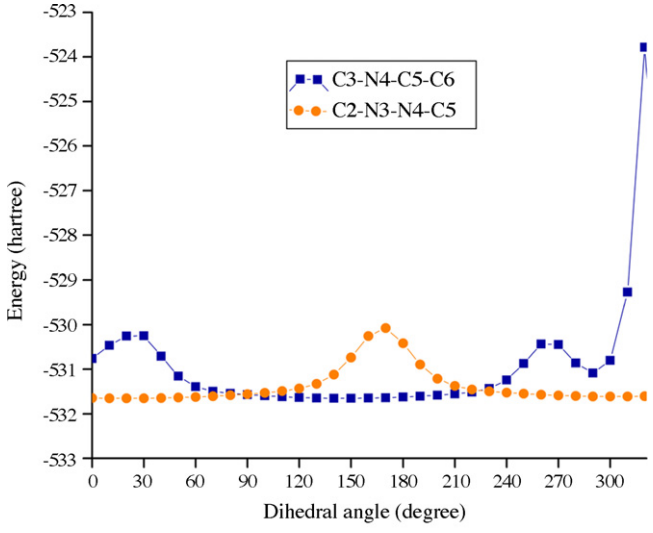

Fig. 3. PES scan for dihedral angles C_2–C_3–N_4–C_5 and C_3–N_4–C_5–C_6 at B3LYP/6-311+G**.

Table 2
Occupation numbers of the interacting NBOs with their respective energies

Parameters	Occupancy (e)			Energy (a.u.)		
	Monomer	Dimer	$\Delta_{occ.}$	Monomer	Dimer	ΔE
$n_1(O_{19})$	1.97380	1.95760	−0.0162	−0.60280	−0.66700	−0.0642
$\sigma^*(C_6{-}O_{20})$	0.05281	0.06484	0.01203	0.64345	0.53974	−0.10371
$\pi^*(C_6{-}O_{20})$	0.40473	0.35862	−0.04611	0.10003	0.06273	−0.0373
$\sigma^*(C_6{-}O_{19})$	0.05387	0.05674	0.00287	0.64292	0.55119	−0.09173
$\sigma^*(C_3{-}N_4)$	0.06310	0.06754	0.00444	0.46714	0.45546	−0.01168
$n_1(O_{15})$	1.97738	1.97739	0.00001	−0.70487	−0.69154	0.01333
$\sigma^*(C_3{-}O_{15})$	0.01606	0.01558	−0.00048	0.52902	0.53395	0.00493
$\pi^*(C_3{-}O_{15})$	0.34768	0.30016	−0.04752	−0.01916	0.00321	0.02237
$n_2(O_{15})$	1.86197	1.86762	0.00565	−0.26231	−0.25196	0.01035
$n_2(O_{19})$	1.83113	1.87786	0.04673	−0.15790	−0.22680	−0.0689
$n_1(O_{20})$	1.97546	1.97433	−0.00113	−0.59153	−0.64292	−0.05139
$n_2(O_{20})$	1.85621	1.86705	0.01084	−0.14574	−0.22361	−0.07787
$\sigma^*(N_{22}{-}H_{23})$	0.02878	0.04078	0.01200	0.29571	0.39056	0.09485
$\sigma^*(N_{22}{-}H_{21})$	0.01225	0.04107	0.02882	0.30039	0.37767	0.07728

experimental values. The calculated bond angles of $N_7{-}C_2{-}C_3$ and $C_2{-}C_3{-}O_{15}$ are lowered by 1.4 and 3.2°, respectively, from the experimental values. The calculated dihedral angles of $C_2{-}C_3{-}N_4{-}C_5$, $C_1{-}C_2{-}C_3{-}O_{15}$ and $C_6{-}C_5{-}N_4{-}H_{16}$ are not equal. The above deviations in the geometrical parameters of L-Ala-Gly between the experimental and theoretical values can be accounted for from the fact that the structure of L-Ala-Gly determined for the solid involves the intermolecular hydrogen bonding whereas the results of the calculations are applicable to the gas phase.

Table 3
Second order perturbation theory analysis of Fock matrix in NBO basis

Donor (i)	Acceptor (j)	$E(2)$[a] (kcal mol^{-1})	$E(j)-E(i)$[b] (a.u.)	$F(i,j)$[c] (a.u.)
Within unit 1				
$n_1(O_{15})$	$\sigma^*(C_3{-}N_4)$	1.59	1.15	0.039
$n_2(O_{15})$	$\sigma^*(C_3{-}N_4)$	21.71	0.71	0.112
$n_1(O_{19})$	$\sigma^*(C_5{-}C_6)$	2.29	1.05	0.044
$n_1(O_{19})$	$\sigma^*(C_6{-}O_{20})$	0.85	1.21	0.029
$n_2(O_{19})$	$\pi^*(C_6{-}O_{20})$	17.26	0.77	0.104
$n_1(O_{19})$	$\sigma^*(N_7{-}H_8)$	6.40	1.06	0.073
$n_2(O_{19})$	$\sigma^*(N_7{-}H_8)$	1.05	0.62	0.023
$n_1(O_{20})$	$\sigma^*(C_5{-}C_6)$	1.21	1.03	0.032
$n_1(O_{20})$	$\sigma^*(C_6{-}O_{19})$	2.39	1.19	0.048
$n_2(O_{20})$	$\sigma^*(C_6{-}O_{19})$	17.79	0.77	0.107
From unit 1 to unit 2				
$n_1(O_{19})$	$\sigma^*(N_{22}{-}H_{23})$	0.51	1.06	0.021
$n_2(O_{19})$	$\sigma^*(N_{22}{-}H_{23})$	0.27	0.63	0.012
$n_1(O_{20})$	$\sigma^*(H_{21}{-}N_{22})$	0.96	1.02	0.028
$n_2(O_{20})$	$\sigma^*(H_{21}{-}N_{22})$	4.93	0.60	0.050
From unit 2 to unit 1				
$n_1(O_{39})$	$\sigma^*(N_7{-}H_{10})$	0.96	1.02	0.028
$n_2(O_{39})$	$\sigma^*(N_7{-}H_{10})$	4.95	0.60	0.050
$n_1(O_{40})$	$\sigma^*(N_7{-}H_8)$	0.49	1.06	0.020
$n_2(O_{40})$	$\sigma^*(N_7{-}H_8)$	0.63	0.62	0.018
Within unit 2				
$n_1(O_{39})$	$\sigma^*(C_{29}{-}C_{30})$	1.21	1.03	0.032
$n_1(O_{39})$	$\sigma^*(C_{30}{-}O_{40})$	2.39	1.19	0.048
$n_2(O_{39})$	$\sigma^*(C_{30}{-}O_{40})$	17.78	0.77	0.107
$n_1(O_{40})$	$\sigma^*(C_{29}{-}C_{30})$	2.28	1.05	0.044
$n_1(O_{40})$	$\sigma^*(C_{30}{-}O_{39})$	0.85	1.21	0.029
$n_2(O_{40})$	$\pi^*(C_{30}{-}O_{40})$	0.54	0.78	0.019

[a] $E(2)$ means energy of hyperconjugative interactions; cf. Eq. (2).
[b] Energy difference between donor and acceptor i and j NBO orbitals.
[c] $F(i,j)$ is the Fock matrix element between i and j NBO orbitals.

Table 4
Definition of internal valence coordinates of L-Ala-Gly

No	Symbol	Type	Definition
Stretching			
1–3	r_i	C—C	C_1—C_2, C_2—C_3, C_5—C_6
4–6	R_i	C—N	C_2—N_7, C_3—N_4, C_5—N_4
7	ϕ_i	N—H	N_4—H_{16}
8	η_i	C—H	C_2—H_{14}
9	q_i	C=O	C_3—O_{15}
10–12	υ_i	C—H (methyl)	C_1—H_{11}, C_1—H_{12}, C_1—H_{13}
13–15	ξ_i	N—H (amino)	N_7—H_8, N7—H_9, N_7—H_{10}
16–17	Q_i	C—H (methylene)	C_5—H_{17}, C_5—H_{18}
18–19	p_i	C—O (carboxyl)	C_6—O_{19}, C_6—O_{20}
Bending			
20–22	β_i	H—C—H (methyl)	H_{13}—C_1—H_{12}, H_{13}—C_1—H_{11}, H_{12}—C_1—H_{11}
23–25	χ_i	C—C—H (methyl)	C_2—C_1—H_{11}, C_2—C_1—H_{12}, C_2—C_1—H_{13}
26–28	α_i	H—N—H (amino)	H_{10}—N_7—H_9, H_{10}—N_7—H_8, H_9—N_7—H_8
29–31	β_i	C—N—H (methyl)	C_2—N_7—H_8, C_2—N_7—H_9, C_2—N_7—H_{10}
32	θ_i	H—C—H (methylene)	H_{17}—C_5—H_{18}
33	π_i	C—C—N	C_6—C_5—N_4
34–35	Υ_i	N—C—H (methylene)	N_4—C_5—H_{18}, N_4—C_5—H_{17}
36–37	π_i	C—C—H (methylene)	C_6—C_5—H_{18}, C_6—C_5—H_{17}
38	ε_i	O—C—O (carboxyl)	O_{19}—C_6—O_{20}
39–40	ε_i	C—C—O	C_5—C_6—O_{19}, C_5—C_6—O_{20}
41–42	σ_i	H—N—C	H_{16}—N_4—C_5, H_{16}—N_4—C_3
43	σ_i	C—N—C	C_5—N_4—C_3
44	φ_i	O—C—N	O_{15}—C_3—N_4
45	φ_i	O—C—C	O_{15}—C_3—C_2
46	φ_i	N—C—C	N_4—C_3—C_2
47–48	δ_i	H—C—C	H_{14}—C_2—C_3, H_{14}—C_2—C_1
49	δ_i	H—C—N	H_{14}—C_2—N_7
50–51	δ_i	N—C—C (amino)	N_7—C_2—C_3, N_7—C_2—C_1
52	δ_i	C—C—C	C_3—C_2—C_1
Out-of-plane			
53	ω_i	C—C	C_5—C_6—O_{20}—O_{19}
54	ω_i	C—O	O_{15}—C_3—N_4—C_2
55	ω_i	N—H	H_{16}—N_4—C_5—C_3
56	ω_i	C—H	H_{14}—C_2—C_3—C_1
Torsion			
57–65	τ_i	tC—CH_3	C_3—C_2—C_1—H_{11}, C_3—C_2—C_1—H_{12}, C_3—C_2—C_1—H_{13}, H_{14}—C_2—C_1—H_{11}, H_{14}—C_2—C_1—H_{12}, H_{14}—C_2—C_1—H_{13}, N_7—C_2—C_1—H_{11}, N_7—C_2—C_1—H_{12}, N_7—C_2—C_1—H_{13}
66–74	τ_i	tC—NH_3	C_3—C_2—N_7—H_8, C_3—C_2—N_7—H_9, C_3—C_2—N_7—H_{10}, H_{14}—C_2—N_7—H_8, H_{14}—C_2—N_7—H_9, H_{14}—C_2—N_7—H_{10}, C_1—C_2—N_7—H_8, C_1—C_2—N_7—H_9, C_1—C_2—N_7—H_{10}
75–80	τ_i	$t$$C_3$—C	N_4—C_3—C_2—H_{14}, N_4—C_3—C_2—C_1, N_4—C_3—C_2—N_7, O_{15}—C_3—C_2—H_{14}, O_{15}—C_3—C_2—C_1, O_{15}—C_3—C_2—N_7
81–84	τ_i	$t$$C_3$—N	C_2—C_3—N_4—C_5, C_2—C_3—N_4—H_{16}, O_{15}—C_3—N_4—C_5, O_{15}—C_3—N_4—H_{16}
85–87	τ_i	tN—CH_2	H_{16}—N_4—C_5—C_6, H_{16}—N_4—C_5—H_{17}, H_{16}—N_4—C_5—H_{18}
88–93	τ_i	$t$$C_5$—C	N_4—C_5—C_6—O_{19}, N_4—C_5—C_6—O_{20}, H_{17}—C_5—C_6—O_{19}, H_{17}—C_5—C_6—O_{20}, H_{18}—C_5—C_6—O_{19}, H_{18}—C_5—C_6—O_{20}

4.2. Potential energy surface (PES) scan studies

The density functional theory (B3LYP/6-311+G**) calculation predicts the energy of the optimized structure in the *cis* conformation is −531.8533 hartrees. The PES scan was performed the torsional angles C_2–C_3–N_4–C_5 and C_3–N_4–C_5–C_6 by using 6-311+G** basis set. The energy curve for the rotations of the dihedrals is presented in Fig. 3. The *cis* conformation of L-Ala-Gly with the dihedral angle C_2–C_3–N_4–C_5 of 0° appears at the minima in the potential energy curve. The energy calculated for the *trans* conformation with the torsional angle C_2–C_3–N_4–C_5 of 170° appears at the maxima. The barrier to this rotation is −530.0756 hartree, which suggests that this rotation is significantly hindered. This relatively large barrier value indicates that the rotation of the methylene group can be attributed to steric effects between the amino groups. The dihedral angle C_3–N_4–C_5–C_6 of 320° appears at the maxima in the potential energy curve. The global minimum has been obtained at the torsional angle 150°. Fig. 3 shows the potential energy curve for the

Table 5
Definition of local symmetry coordinates (much like the natural internal coordinates) and the corresponding force constant (mdyn/Å) with scale factors used

No	Symbol	Definition	Force constant	Scale factors
1–3	CC st	r_1, r_2, r_3	4.17	0.899
4–6	C—N st	R_4, R_5, R_6	3.12	0.899
7	NH st	ϕ_7	4.77	0.861
8	CH st	η_8	4.77	0.899
9	CO st	q_9	11.09	0.899
10	CH_3 ss	$(\upsilon_{10} + \upsilon_{11} + \upsilon_{12})/\sqrt{3}$	42.86	0.888
11	CH_3 ips	$(2\upsilon_{10} + \upsilon_{11} + \upsilon_{12})/\sqrt{6}$	43.21	0.888
12	CH_3 ops	$(\upsilon_{11} - \upsilon_{12})/\sqrt{2}$	4.70	0.888
13	NH_3 ss	$(\xi_{13} + \xi_{14} + \xi_{15})/\sqrt{3}$	50.31	0.888
14	NH_3 ips	$(2\xi_{13} + \xi_{14} + \xi_{15})/\sqrt{6}$	47.61	0.888
15	NH_3 ops	$(\xi_{14} - \xi_{15})/\sqrt{2}$	5.91	0.888
16	CH_2 ss	$(Q_{16} + Q_{17})/\sqrt{2}$	4.65	0.92
17	CH_2 ips	$(Q_{16} - Q_{17})/\sqrt{2}$	4.54	0.92
18	COO ss	$(p_{18} + p_{19})/\sqrt{2}$	11.28	0.92
19	COO ips	$(p_{18} - p_{19})/\sqrt{2}$	9.14	0.92
20	CH_3 sb	$(\beta_{20} + \beta_{21} + \beta_{22} - \chi_{23} - \chi_{24} - \chi_{25})/\sqrt{6}$	0.58	0.948
21	CH_3 ipb	$(2\beta_{20} - \beta_{21} - \beta_{22})/\sqrt{6}$	0.56	0.948
22	CH_3 opb	$(\beta_{21} - \beta_{22})/\sqrt{2}$	0.55	0.948
23	CH_3 ipr	$(2\chi_{23} - \chi_{24} - \chi_{25})/\sqrt{6}$	0.59	0.863
24	CH_3 opr	$(\chi_{24} - \chi_{25})/\sqrt{2}$	0.61	0.863
25	NH_3 sb	$(\alpha_{26} + \alpha_{27} + \alpha_{28} - \beta_{29} - \beta_{30} - \beta_{31})/\sqrt{6}$	0.55	0.911
26	NH_3 ipb	$(2\alpha_{26} - \alpha_{27} - \alpha_{28})/\sqrt{6}$	2.44	0.911
27	NH_3 opb	$(\alpha_{27} - \alpha_{28})/\sqrt{2}$	2.48	0.911
28	NH_3 ipr	$(2\beta_{29} - \beta_{30} - \beta_{31})/\sqrt{6}$	0.65	0.918
29	NH_3 opr	$(\beta_{30} - \beta_{31})/\sqrt{2}$	0.59	0.918
30	CH_2 sci	$(5\theta_{32} + \pi_{33})/\sqrt{26}$	0.80	0.931
31	NCC sci	$(\theta_{32} + 5\pi_{33})/\sqrt{26}$	2.11	0.931
32	CH_2 rok	$(\Upsilon_{34} - \pi_{36} + \Upsilon_{35} - \pi_{37})/2$	0.68	0.931
33	CH_2 wag	$(\Upsilon_{34} + \Upsilon_{35} - \pi_{36} - \pi_{37})/2$	0.61	0.931
34	CH_2 twi	$(\Upsilon_{34} + \Upsilon_{35} - \pi_{37} - \pi_{36})/2$	0.62	0.931
35	COO sb	$(2\varepsilon_{38} - \varepsilon_{39} - \varepsilon_{40})/\sqrt{6}$	1.26	0.931
36	COO rok	$(\varepsilon_{39} - \varepsilon_{40})/\sqrt{2}$	1.28	0.931
37	NH rok	$(\sigma_{41} - \sigma_{42})/\sqrt{2}$	0.54	0.91
38	CNC df	$(2\sigma_{43} - \sigma_{41} - \sigma_{42})/\sqrt{6}$	0.99	0.91
39	CO rok	$(\varphi_{44} - \varphi_{45})/\sqrt{2}$	1.0	0.833
40	CCN df	$(2\varphi_{46} + \varphi_{44} - \varphi_{45})/\sqrt{6}$	1.62	0.833
41	CH ipr	$(2\delta_{47} - \delta_{48} - \delta_{49})/\sqrt{6}$	1.78	0.962
42	CH opr	$(\delta_{48} - \delta_{49})/\sqrt{2}$	4.02	0.962
43	NCC asdf	$(2\delta_{50} - \delta_{51} - \delta_{52})/\sqrt{6}$	4.58	1.003
44	NCC asdfo	$(2\delta_{51} - \delta_{50} - \delta_{52})/\sqrt{6}$	4.03	1.003
45	CC wag	ω_{53}	0.35	0.91
46	CO wag	ω_{54}	0.51	0.833
47	NH wag	ω_{55}	0.16	0.91
48	CH wag	ω_{56}	6.65	1.197
49	$t\mathrm{CH_3}$	$(\tau_{57} + \tau_{58} + \tau_{59} + \tau_{60} + \tau_{61} + \tau_{62} + \tau_{63} + \tau_{64} + \tau_{65})/3$	0.01	0.929
50	$t\mathrm{NH_3}$	$(\tau_{66} + \tau_{67} + \tau_{68} + \tau_{69} + \tau_{70} + \tau_{71} + \tau_{72} + \tau_{73} + \tau_{74})/3$	0.02	1.009
51	$t\mathrm{C_3C}$	$(\tau_{75} + \tau_{76} + \tau_{77} + \tau_{78} + \tau_{79} + \tau_{80})/\sqrt{6}$	0.08	1.009
52	$t\mathrm{C_3N}$	$(\tau_{81} + \tau_{82} + \tau_{83} + \tau_{84})/2$	0.05	0.953
53	$t\mathrm{CH_2}$	$(\tau_{85} + \tau_{86} + \tau_{87})/\sqrt{3}$	0.12	1.009
54	$t\mathrm{C_5C}$	$(\tau_{88} + \tau_{89} + \tau_{90} + \tau_{91} + \tau_{92} + \tau_{93})/\sqrt{6}$	0.03	1.009

dihedral angle C_3—N_4—C_5—C_6 has a flat region extending from 120 to 200°. In the vicinity of the torsional angle of 150° L-Ala-Gly possesses the non-planarity of the peptide group.

4.3. Natural bond orbital analysis

The natural bonding orbitals (NBO) calculations [18] were performed using NBO 3.1 program as implemented in the Gaussian 98 package at the DFT/B3LYP level in order to understand various second order interactions between the filled orbitals of one subsystem and vacant orbitals of another subsystem, which is a measure of the intermolecular delocalization or hyperconjugation. NBO analysis provides the most accurate possible 'natural Lewis structure' picture of *j*, because all orbital details are mathematically chosen to include the highest possible percentage of the electron density. A useful aspect of the NBO method is that it gives information about interactions in both filled and virtual orbital spaces that could enhance the analysis of intra- and intermolecular interactions.

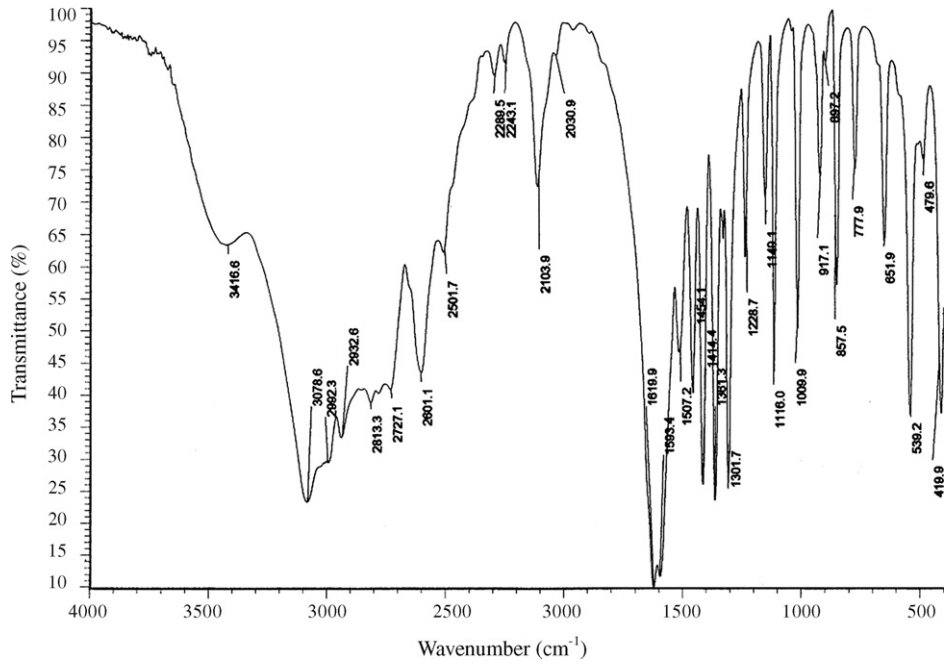

Fig. 4. FT-IR spectrum of L-Ala-Gly in the wavenumber range 4000–400 cm^{-1}.

The second order Fock matrix was carried out to evaluate the donor–acceptor interactions in the NBO basis [19]. The interactions result in a loss of occupancy from the localized NBO of the idealized Lewis structure into an empty non-Lewis orbital. For each donor (i) and acceptor (j), the stabilization energy $E(2)$ associated with the delocalization $i \rightarrow j$ is estimated as

$$E(2) = \Delta E_{ij} = q_i \frac{F(i,j)^2}{\varepsilon_j - \varepsilon_i}, \quad (2)$$

where q_i is the donor orbital occupancy, ε_i and ε_j are diagonal elements and $F(i,j)$ is the off diagonal NBO Fock matrix element.

The NBO analysis of L-Ala-Gly in comparison between monomer and dimer clearly explains the evidences of the formation of strong H-bonded interaction between oxygen lone electron pairs and σ^*(N–H) antibonding orbitals. The importance of hyperconjugation and electron density transfer from lone electron pairs of the Y atom to the X—H antibonding orbital in the X—H···Y system has been reported

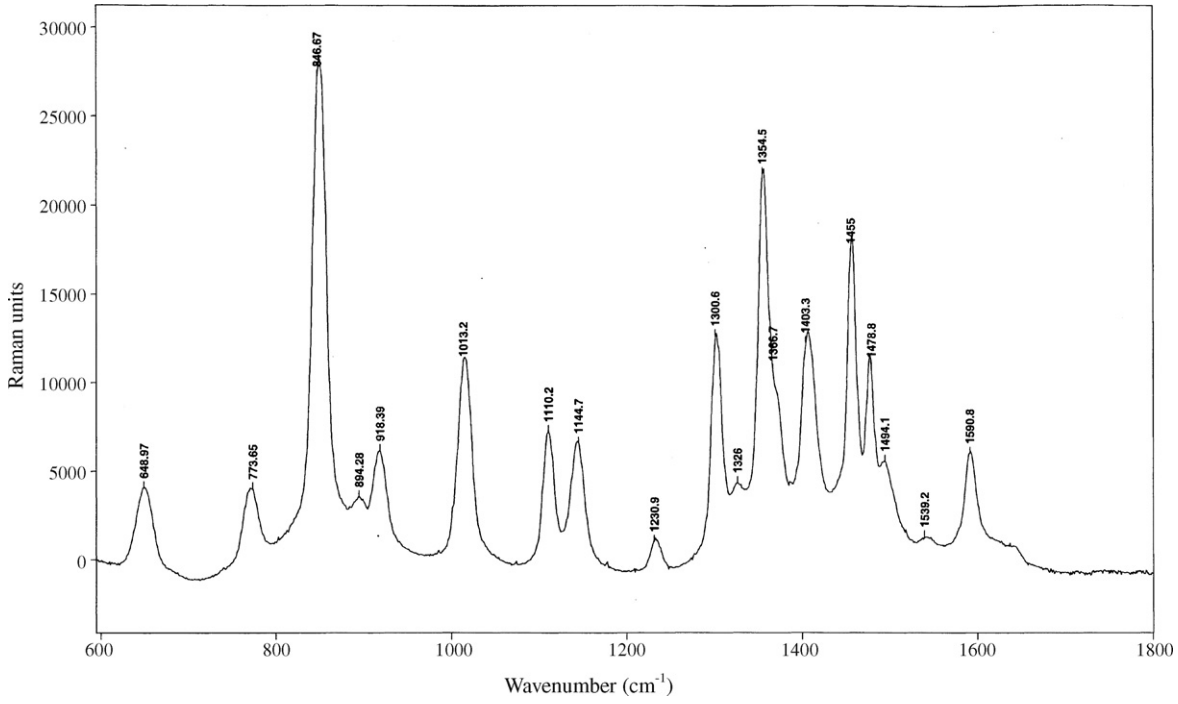

Fig. 5. Raman spectrum of L-Ala-Gly in the wavenumber range 600–1800 cm^{-1}.

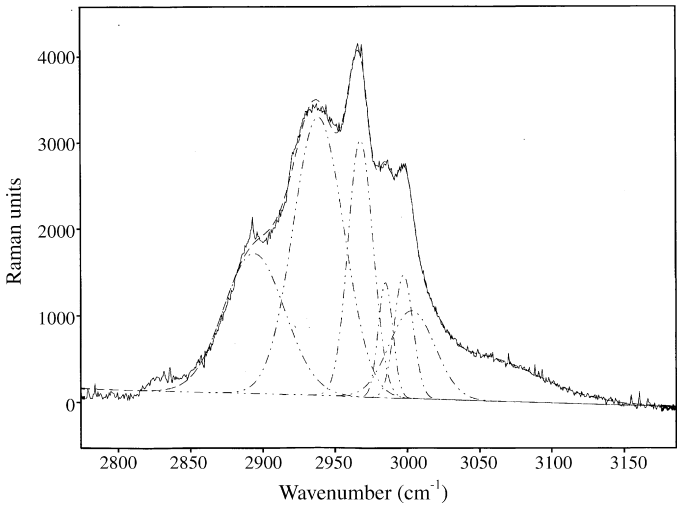

Fig. 6. Raman spectrum of L-Ala-Gly in the wavenumber range 2750–3200 cm^{-1}.

[20]. In general such interaction leads to an increase in population of X—H antibonding orbital. In Table 2, the magnitudes of charges transferred from lone pairs of (n_{19}) and (n_{20}) of the hydrogen bonded O atoms into the antibonds $\sigma^*(N_{22}–H_{23})$ and σ^* $(N_{22}–H_{21})$ being the H donors, respectively, was significantly increased 0.012 and 0.029 e upon dimerization providing clear evidence about the weakening of both N–H bonds, which contribute to the elongation of their bonds and red shifts of corresponding stretching frequencies. The stabilization energy $E(2)$ coupled with hyperconjugative interactions $n_1(O_{19}) \rightarrow \sigma^*(N_{22}–H_{23})$, $n_2(O_{19}) \rightarrow \sigma^*(N_{22}–H_{23})$, $n_1(O_{20}) \rightarrow \sigma^*(N_{22}–H_{21})$ and $n_2(O_{20}) \rightarrow \sigma^*(N_{22}–H_{21})$ are obtained as 0.51, 0.96, 0.27, and 4.93 kcal mol^{-1}, respectively (Table 3) which enumerate the extend of intermolecular hydrogen bonding. The differences in energies are reasonably owing to the fact that the accumulation of electron density in the N—H bond is not only drawn from the n(O) of hydrogen acceptor but also from the entire molecule.

4.4. Spectral analysis

The vibrational band assignments have been made based on normal coordinate analysis. Internal coordinates have been chosen according to Pulay's recommendations [21]. The complete sets of internal coordinates for L-Ala-Gly are given in Table 4. Moreover, the selective scaling was incorporated according to the SQM procedure using a set of 17 transferable scale factors (Table 5) recommended by Rauhut and Pulay [12]. The SQM frequencies related to the observed peaks are shown in Table 6 along with detailed assignments. The assigned frequencies as predicted from the basis sets B3LYP/6-31G* and 6-31G11+G** is nearly same except for slight variations in the potential energy distributions. The observed and simulated FT-IR and Raman spectra of L-Ala-Gly are given in Figs. 4–8. The complete vibrational assignments are given in Table 6.

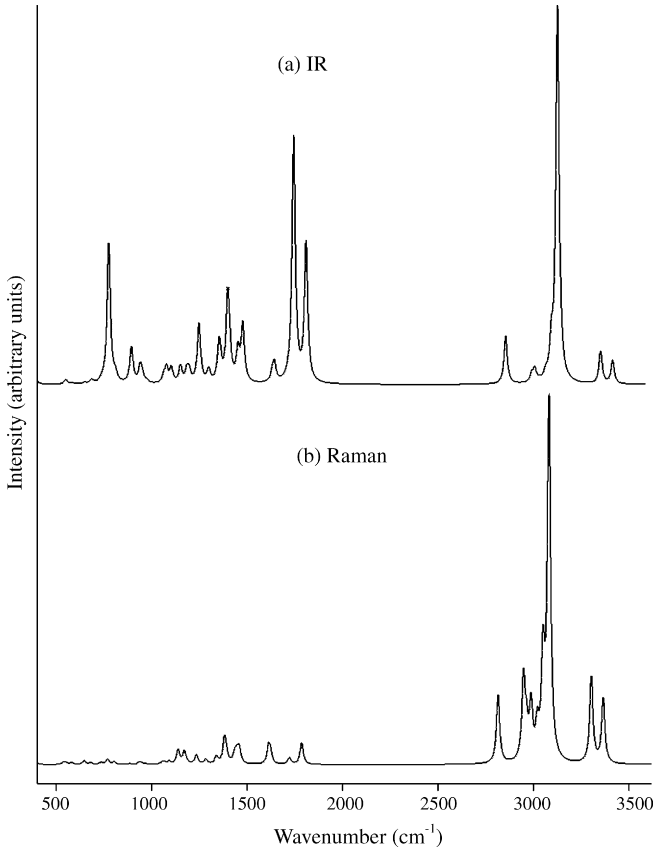

Fig. 7. Simulated (a) IR and (b) Raman spectra of L-Ala-Gly in the wavenumber range 400–3500 cm^{-1} at B3LYP/6-31G* level.

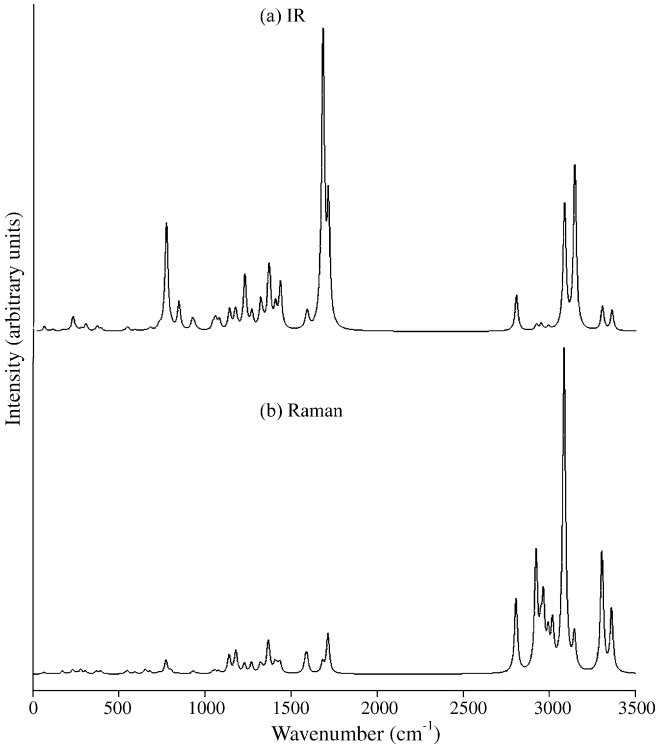

Fig. 8. Simulated (a) IR and (b) Raman spectra of L-Ala-Gly in the wavenumber range 400–3500 cm^{-1} at B3LYP/6-311+G** level.

Table 6
Vibrational assignment of L-Ala-Gly by normal mode analysis based on SQM force field calculations

Observed fundamentals (cm^{-1})		Selective scaled force field				
ν_{IR}	ν_{Raman}	ν_i cm^{-1}		A_i IR[a]	I_i R[b]	Assignment with PED (%)[c]
		B3LYP/6-31G*	B3LYP/6-311+G**			
3417 s br						H_2O absorption
3078 s		3296	3296	53.7	87.4	NH_3 ops (100)
2992 s	2998 w	3236	3242	74.1	116.9	NH_3 ss (74), NH_3 ips (26)
	2986 w	3017	3033	655.8	536.1	NH_3 ips (61), NH_3 ss (39)
	2966 m	2960	2961	113.7	36.9	CH_2 ips (35), CH_2 ss (20), NH (13), CH_3 ops (12)
2933 s	2937 w	2958	2959	35.2	29.8	CH_3 ops (39), CH_3 ips (22), CH_3 ss (17), CH (12)
		2941	2943	30.4	50.6	CH (53), CH_3 ops (14)
	2893 w	2887	2866	19.4	110.2	CH_3 ss (58), CH_3 ips (42)
2813 s	2857 w	2805	2815	123.4	100.4	CH_2 ss (45), CH_2 ips (25), NH_3 ips (19), NH_3 ss (11)
	1786 vw	1781	1720	345.9	29.2	CO (62), CN (18)
1620 vs		1700	1672	543.3	8.1	COO ips (88)
		1610	1613	42.4	14.2	NH_3 opb (84), NH_3 ipb (13)
1593 s sh	1591 m	1599	1603	21.8	22.6	NH_3 ipb (64), NH_3 opb (33)
1507 m	1494 m sh	1470	1468	12.6	12.9	CH_3 opb (87)
	1479 s	1461	1456	89.6	5.0	NH_3 sb (47), CH_2 sci (38)
1454 s	1455 s	1452	1454	8.5	12.4	COO ss (67), CH wag (11)
1414 s		1434	1413	79.5	12.3	CH_2 sci (44), NH_3 sb (30)
	1403 s	1407	1408	37.6	7.8	CH_3 sb (72)
1361 s	1367 m sh	1368	1361	217.2	36.6	CN (29), NH rok (28), CO (10)
	1354 vs	1362	1367	8.0	3.9	CH wag (49), CH opr (48)
	1326 w	1330	1325	93.0	7.6	CH ipr (31), CH wag (27)
1302 s	1301 s	1277	1272	36.0	8.9	CH ipr (33), CH wag (29), COO ss (14)
1229 m	1231 w	1226	1229	113.3	11.1	CH wag (23), CH ipr (21), NH rok (18)
		1193	1190	40.9	1.5	NH_3 ipr (18), NCC df2 (11), NH_3 ipb (10), CC (10)
1149 m	1145 m	1137	1144	44.5	19.3	CH_2 wag (44), CH_2 twi (19)
1116 s	1110 m	1103	1096	11.4	4.5	CH ipr (27), CH wag (20), NH_3 opr (14)
		1071	1065	59.6	3.5	CN (36)
1010 s	1013 s	1034	1043	14.0	2.1	CH_3 ipr (17), CC (17), CH wag (16), CN (12), CH_3 opr (11), NCC df1 (11)
	964 vw	966	960	4.0	1.0	CH_2 rok (68), CC wag (16)
	941 w	930	924	28.1	2.3	CC (27), NH_3 ipr (21), CH_3 opr (13)
917 m	918 m	917	914	31.5	2.4	CH opr (33), CH wag (15), CH_3 opr (11), NH_3 ipr (10)
897 w sh	894 w	895	893	74.4	1.0	NCt (39), NH wag (20), C3Nt (13)
857 s	847 vs	795	799	13.4	4.0	CN (34), CH wag (27)
778 m	774 m	768	772	321.5	6.8	COO sb (56), CC (34)
727 w sh		730	732	7.2	2.3	CC (24), CO wag (14), NCC df1 (12)
	679 w	666	671	12.1	1.5	NCC sci (16), CO wag (12), CO rok (11), CC (10)
652 m	649 m	639	651	3.3	6.4	CC (23), CN (18)
584 w		578	593	3.0	2.6	CC wag (60), CH_2 rok (18), NCt (10)
539 s		539	549	8.8	3.4	COO rok (19), CC (18), CO rok (11), CO wag (10), CNC def (10)
479 vw		529	534	1.8	1.7	CCN def (29), NCC df1 (21), CC (17)
420 s		385	388	22.0	5.7	COO rok (29), CH wag (23), CC (10)

vs, very strong; s, strong; m, medium; sh, shoulder; w, weak; vw, very weak; br, broad; st, stretching; t, torsion; ss, symmetric stretching; ips, in plane stretching; ops, out of plane stretching; ipb, in plane bend; opb, out of plane bend; sb, symmetric bending; sci, scissoring; wag, wagging; twi, twisting; rok, rocking; ipr, in plane rocking; opr, out of plane rocking; df, deformation; asdf, asymmetric deformation; asdfo, out of plane asymmetric deformation.

[a] Calculated IR intensities.

[b] Relative Raman intensities normalized to 100 cf. Eq. (1).

[c] Only PED values greater than 10% are given.

4.5. NH_3^+ group vibrations

The zwitterionic form of dipeptides, the NH_3^+ asymmetric and symmetric stretching band appears in the region 3330 and 3080 cm^{-1}, respectively [22]. The observed broad intense IR band at 3078 cm^{-1} corresponds to NH_3^+ asymmetric stretching mode. The strong band at 2992 cm^{-1} in IR and a weak band at 2998 cm^{-1} in Raman are attributed to NH_3^+ symmetric stretching mode. The lowering of NH_3^+ stretching wave numbers indicate the formation of both inter- and intramolecular hydrogen bonding of the NH_3^+ group with COO^- ion. The N–H···O distances (Table 7) supports the existence of N–H···O

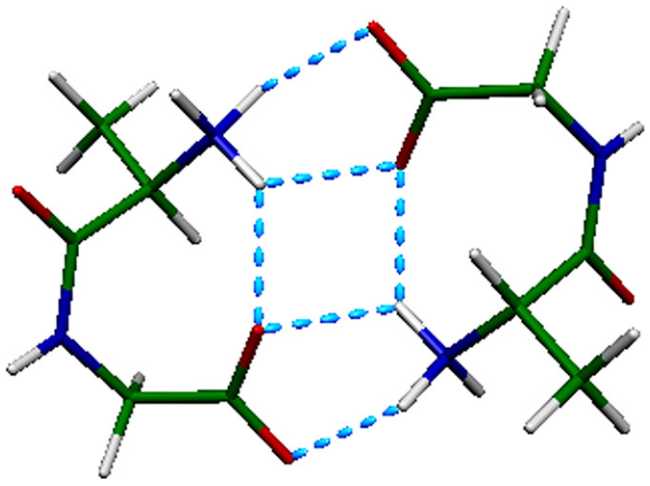

Fig. 9. Hydrogen bonding structure of L-Ala-Gly dimer.

hydrogen bonds in the molecule. The inter- and intramolecular N–H···O hydrogen bonding structure of L-Ala-Gly-dimer is shown in Fig. 9.

4.6. Methyl and methine group vibrations

The stretching vibrations of the CH_3 and CH group of alanine and glycine are assigned as a number of sharp bands in the region 2980–2875 cm^{-1} [23]. The asymmetrical CH_3 stretching is observed in IR as a strong band at 2933 cm^{-1} and a weak band at 2937 cm^{-1} in Raman. The symmetric methyl stretching mode is assigned as a weak band at 2893 cm^{-1} in Raman spectrum. The out of plane bending vibrations are observed at 1507 and 1494 cm^{-1} in IR and Raman, respectively. The strong band in IR at 1454 cm^{-1} is attributed to the methyl in plane bending mode. The Raman counterpart is observed at the same wavenumber with strong intensity. NCA predicts in the region 2941 cm^{-1} is assigned as the CH stretching mode. Freedman et al. [24] have assigned the methine bending modes of Gly-L-Ala zwitterion at 1330 and 1286 cm^{-1} in the vibrational circular dichroism spectra. In L-Ala-Gly, the CH deformation vibrations are observed as the strong bands at 1354 and 1301 cm^{-1} and a weak band at 1326 cm^{-1} in Raman. In IR spectrum, the corresponding mode is assigned as a strong intense band at 1302 cm^{-1}.

4.7. Methylene vibrations

Dipolar forms (H_3N^+–CH_2–COO^-) of the glycine molecule, the CH_2 stretching modes are appear in the region 2975 and 3011 cm^{-1} [25]. In L-Ala-Gly, the asymmetric stretching mode of methylene group is observed as a medium intense band in Raman at 2966 cm^{-1} and the symmetric stretching vibration is assigned at 2813 cm^{-1} in IR and a week band at 2857 cm^{-1} in Raman. In NCA, these stretching modes are predicted at 2958 (at B3LYP/6-31G*) and 2805 cm^{-1} (6-311+G**). The CH_2 scissoring mode is observed as a strong band in Raman at 1403 cm^{-1} which is coupled with NH_3^+ bending vibrations. The methylene wagging vibration assigned as medium bands at 1149 cm^{-1} (IR) and 1145 cm^{-1} (Raman).

Table 7
Hydrogen bonding geometry of L-Ala-Gly-dimer (Å, °)

D–H···A	D–H	H···A	D···A	D–H···A
N_7–H_{10}···O_{39}	1.08	1.62	2.68	166.69
N_7–H_8···O_{40}	1.41	2.96	3.03	83.50
N_7–H_8···O_{19}	1.05	1.76	2.74	153.93
N_{22}–H_{23}···O_{19}	1.05	1.82	2.70	138.50
N_{22}–H_{21}···O_{20}	1.04	1.88	2.67	130.31
N_{22}–H_{23}···O_{40}	1.06	1.69	2.69	155.44

4.8. Carboxylic and carbonyl vibrations

The unionized carboxylic group stretching frequencies are occurring in the region 1700–1730 cm^{-1}. The ionized carboxylic group COO^- asymmetric and symmetric stretching wave numbers are expected in the region 1560–1600 cm^{-1} and 1410 cm^{-1}, respectively [26,27]. The strong intense band in IR at 1620 cm^{-1} is assigned as COO^- asymmetric stretching. The symmetric stretching mode is observed at 1454 cm^{-1} in IR. The Raman counterpart is observed as a strong band at 1455 cm^{-1}. These observations indicate the ionized carboxylic group is present in the molecule. Moreover, the C=O stretching mode of the amide group is observed as a weak band in Raman at 1786 cm^{-1}. The predicted C=O stretching mode (1781 cm^{-1}) is very close to the expected results.

5. Conclusions

A complete vibrational analysis of L-Ala-Gly was performed using B3LYP density functional theory calculations. The molecular structure is conformed theoretically as non-planarity of the peptic group. The PES scan studies also support the non-planarity. The shorting of C_3–O_{15} bond length and the increasing of N_4–C_3–O_{15} bond angle shows that the oxygen of the peptic group is not implemented in any hydrogen link. The normal coordinate analysis predicts a good agreement between the observed and calculated frequencies. The various modes of vibrations were unambiguously assigned on the results of PED output obtained from the normal coordinate analysis. The assignment of the fundamentals was confirmed by the qualitative agreement between the calculated and observed band intensities and polarization properties as well and is observed to be unambiguous. The lowering of NH_3^+ stretching wavenumber is due to the formation of strong N–H···O hydrogen bonding between the NH_3^+ and COO^- groups. The hydrogen bonding networks has been thoroughly analyzed using NBO analysis. Second order perturbation theory results shows that the transfer of ED from the lone pair oxygen to the antibonding orbital of N–H bond produces strong evidences of N–H···O hydrogen bonds.

Acknowledgement

The authors thank Professor Tom Sundius, Department of Physical Sciences, University of Helsinki, Helsinki, Finland, for providing the MOLVIB software.

References

[1] S. Karim, J. Bandekar, J. Adv. Protein Chem. 38 (1986) 181.
[2] J.H. Caldwell, N.W. Daw, H.J. Wyatt, J. Physiol. 276 (1978) 277.
[3] George A. Jefferey, An Introduction to Hydrogen Bonding, Oxford University Press, Oxford, 1997.
[4] P.J. Greenstein, M. Winitz, Chemistry of the Amino Acids, Wiley, New York, 1961.
[5] H.D. Mootz, M.A. Marahiel, Curr. Opin. Biotechnol. 10 (1999) 341.
[6] C. James, A. Amal Raj, R. Reghunathan, V.S. Jayakumar, I. Hubert Joe, J. Raman Spectrosc. 37 (2006) 1381.
[7] M. Enrique, Cabaleiro-Lago, Miguel A. Rios, J. Chem. Phys. 113 (2000) 9523.
[8] Michel H.J. Koch, G. Germain, Acta Crystallogr. B 26 (1970) 410.
[9] Mary Virginia Orna, Enzymes: Biochemical Catalysts, A Source Book Module, Version 1.0, 1993.
[10] M.J. Frisch, G.W. Trucks, H.B. Schlegel, G.E. Scuseria, M.A. Robb, J.R. Cheeseman, V.G. Zakrzewski, J.A. Montgomery Jr., R.E. Stratmann, J.C. Burant, S. Dapprich, J.M. Millam, A.D. Daniels, K.N. Kudin, M.C. Strain, O. Farkas, J. Tomasi, V. Barone, M. Cossi, R. Cammi, B. Mennucci, C. Pomelli, C. Adamo, S. Clifford, J. Ochterski, G.A. Petersson, P.Y. Ayala, Q. Cui, K. Morokuma, D.K. Malick, A.D. Rabuck, K. Raghavachari, B. Foresman, J. Cioslowski, J.V. Ortiz, A.G. Baboul, B.B. Stefanov, G. Liu, A. Liashenko, P. Piskorz, I. Komaromi, R. Gomperts, R.L. Martin, D.J. Fox, T. Keith, M.A. Al-Laham, C.Y. Peng, A. Nanayakkara, M. Challacombe, P.M.W. Gill, B. Johnson, W. Chen, M.W. Wong, J.L. Andres, C. Gonzalez, M. Head-Gordon, E.S. Replogle, J.A. Pople, Gaussian 98, Revision A9, Gaussian, Inc., Pittsburgh, PA, 1998.
[11] P. Pulay, G. Fogarasi, G. Pongor, J.E. Boggs, A. Vargha, J. Am. Chem. Soc. 105 (1983) 7037.
[12] G. Rauhut, P. Pulay, J. Phys. Chem. 99 (1995) 3093.
[13] J.B. Foresman, A. Frisch, Exploring Chemistry with Electronic Structure Methods, 2nd ed., Gaussian, Inc., Pittsburgh, PA, 1996.
[14] T. Sundius, J. Mol. Struct. 218 (1990) 321.
[15] T. Sundius, Vib. Spectrosc. 29 (2002) 89.
[16] G. Keresztury, S. Holly, J. Varga, G. Besenyei, A.Y. Wang, J.R. Durig, Spectrochim. Acta 49A (1993) 2007.
[17] G. Keresztury, in: J.M. Chalmers, P.R. Griffith (Eds.), Raman Spectroscopy: Theory in Handbook of Vibrational Spectroscopy, vol. 1, John Wiley & Sons Ltd., New York, 2002.
[18] E.D. Glendening, A.E. Reed, J.E. Carpenter, F. Weinhold, NBO Version 3.1, TCI, University of Wisconsin, Madison, 1998.
[19] A.E. Reed, L.A. Curtiss, F. Weinhold, Chem. Rev. 88 (1988) 899.
[20] J. Chocholousova, V. Vladimir Spirko, P. Hobza, Phys. Chem. Chem. Phys. 6 (2004) 37.
[21] P. Pulay, G. Fogarasi, F. Pang, J.E. Boggs, J. Am. Chem. Soc. 101 (1979) 2550.
[22] L.J. Bellamy, The Infra-red Spectra of Complex Molecules, John Wiley and Sons, Inc., New York, 1975.
[23] M.K. Mohammady, K.J. Jalkanen, N. Nardi, R.C. Wade, S. Suhai, Chem. Phys. 240 (1999) 63.
[24] T.B. Freedman, A.C. Chernovitz, W.M. Zuk, G. Paterlini, L.A. Nafie, J. Am. Chem. Soc. 110 (1988) 6970.
[25] F.R. Dollish, W.G. Fateley, F.F. Bentley, Characteristic Raman Frequencies of Organic Compounds, John Wiley and Sons, Inc., New York, 1974.
[26] I. Hubert Joe, G. Aruldhas, S. Anbu kumar, P. Ramasamy, J. Cryst. Res. Technol. 29 (1994) 685.
[27] I.D. Reva, S.G. Stepanian, A.M. Plokhotnichenko, E.D. Radchenko, G.G. Sheina, Yu.P. Blagoi, J. Mol. Struct. 318 (1994) 1.